Check for updates

EurJIC
European Journal of Inorganic Chemistry

A Journal of ChemPubSoc Europe

Accepted Article

Title: Bimetallic Ag-Au nanoparticles inside mesoporous titania thin films: synthesis by photoreduction, and galvanic replacement and catalytic activity

Authors: Rusbel Coneo Rodríguez, Horacio Troiani, Sergio E. Moya, Mariano M. Bruno, and Paula Cecilia Angelomé

This manuscript has been accepted after peer review and appears as an Accepted Article online prior to editing, proofing, and formal publication of the final Version of Record (VoR). This work is currently citable by using the Digital Object Identifier (DOI) given below. The VoR will be published online in Early View as soon as possible and may be different to this Accepted Article as a result of editing. Readers should obtain the VoR from the journal website shown below when it is published to ensure accuracy of information. The authors are responsible for the content of this Accepted Article.

To be cited as: *Eur. J. Inorg. Chem.* 10.1002/ejic.201901186

Link to VoR: http://dx.doi.org/10.1002/ejic.201901186

WILEY-VCH

10.1002/ejic.201901186

Bimetallic Ag-Au nanoparticles inside mesoporous titania thin films: synthesis by photoreduction and galvanic replacement, and catalytic activity

Dr. Rusbel Coneo Rodríguez[a,b], Dr. Horacio Troiani[c], Dr. Sergio E. Moya[d], Dr. Mariano M. Bruno[b], Dr. Paula C. Angelomé[a]*

(a) Gerencia Química & Instituto de Nanociencia y Nanotecnología, Centro Atómico Constituyentes, Comisión Nacional de Energía Atómica, CONICET, Av. Gral. Paz 1499, B1650KNA, San Martín, Buenos Aires, Argentina.
(b) Departamento de Química, Universidad Nacional de Río Cuarto, CONICET, X5804BYA, Río Cuarto, Córdoba, Argentina.
(c) Departamento de Caracterización de Materiales, GIA, CONICET, Centro Atómico Bariloche, Comisión Nacional de Energía Atómica, 8400 San Carlos de Bariloche, Río Negro, Argentina.
(d) CIC biomaGUNE, Paseo de Miramón 182, 20014 Donostia-San Sebastián, Spain

* Corresponding author, email: angelome@cnea.gov.ar, webpage: www.qnano.com.ar

Accepted Manuscript

This article is protected by copyright. All rights reserved.

Abstract

In this work, the synthesis and catalytic activity of bimetallic Ag-Au nanoparticles (NPs) supported in TiO_2 mesoporous thin films (MTF) are presented. The composite materials were obtained through a two-step procedure, performed at room conditions. In the first step, Ag NPs were grown inside the MTF by photoreduction. Then, a galvanic replacement reaction with Au was carried out, yielding the bimetallic NPs. The composites were characterized by UV–vis spectroscopy, transmission electron microscopy (TEM), X-ray photoelectron spectroscopy (XPS) and X-ray reflectometry (XRR), which show that the alloyed Ag-Au NPs are present inside the mesopores. Moreover, Ag and Au composition relationship can be controlled by adjusting the reaction times of the photoreduction and galvanic replacement reactions, respectively. Pores remain accessible after NPs synthesis, a feature that ensures their possible applications in any device that requires the contact between the NPs and the medium. Catalytic activity of the composites towards 4-nitrophenol reduction by sodium borohydride was evaluated. Although all the bimetallic systems exhibit improved catalytic properties in comparison with the monometallic Ag composite, the sample with lower Au-Ag relationship is the most effective. For the first time, to the best of our knowledge, bimetallic Au-Ag NPs are encapsulated inside mesoporous TiO_2 films, paving the way towards a wide variety of applications.

Keywords

Bimetallic nanoparticles; mesoporous thin film; TiO_2; galvanic replacement; catalysis

Accepted Manuscript

This article is protected by copyright. All rights reserved.

Introduction

Metallic nanoparticles (NPs) have unique optical and catalytic properties resulting from their high surface to volume ratio and their easily tunable sizes and shapes.[1] These properties make metallic NPs attractive for a wide variety of applications in very diverse fields such as plasmonic sensing, optoelectronics, bioimaging and catalysis. In the last decades, a way to tune NPs properties has been developed by means of combining different metals in a nanoparticle, the so called bimetallic NPs.[2] The chemical and physical properties of bimetallic NPs are unique in comparison to monometallic and bulk metal alloys, due to the synergistic effects derived from the combination of different metals.[3] In fact, bimetallic NPs show excellent characteristics for applications in the fields of optics,[4] electrochemistry,[5] electroanalytic,[5] bioelectrochemistry,[6] biosensing,[7] and catalysis.[8],[9]

Among bimetallic NPs, the Au–Ag metal nanostructures have been extensively explored due to their simple synthesis procedures and their tunable localized surface plasmon resonance (LSPR) bands in the visible region.[2] The formation of such bimetallic composites helps to overcome the poor chemical and structural stability of Ag NPs, that have limited their practical applications.[10] Nanoparticles with high stability and excellent properties can be obtained by alloying Ag with chemically inert Au.[10] Au-Ag bimetallic nanostructures include alloys and core-shell NPs such as Ag@Au and Au@Ag, and have been employed successfully as catalysts[11] and SERS substrates.[12] In most cases, such bimetallic NPs were obtained in colloidal solutions, limiting their uses. A step further in the design of bimetallic NPs is to use a support in order to confine the particles, increment their stability and avoid their aggregation under operation conditions. Among all the proposed supports,[13] mesoporous oxides are very promising since they present a high specific area and well-defined monodisperse mesopores with diameters in the 2-50 nm range in which NPs can be formed.[14] Such oxides are obtained by the combination of sol-gel chemistry, used to generate the inorganic framework, and self-assembly of amphiphilic molecules, that act as pores template. A characteristic well-ordered array of mesopores is obtained after template removal by either calcination or solvent extraction.[15] There are several examples in the literature of the use of these oxides as supports for bimetallic nanoparticles, not only to prevent aggregation and improve the NPs stability, but also to enhance their catalytic activity.[14a, 16] Interestingly, most of reported the bimetallic composites are based on colloidal mesoporous SiO_2, a very inert oxide that, in principle,

Accepted Manuscript

This article is protected by copyright. All rights reserved.

does not interact with the supported NPs. In many cases functionalization of the oxide structure was necessary to ensure the NPs formation.

Having in mind the applications of the bimetallic NPs – mesoporous oxides composites, preparing them as thin films has several advantages. In fact, mesoporous thin films can be synthesized on top of almost any flat substrate. They can be designed to be partially transparent in the visible region, are portable and can be easily introduced and extracted from reaction media. Moreover, they may be integrated inoptoelectronical devices.[17] Several examples of composite materials obtained by combining pure metallic NPs and mesoporous thin films (MTF) have been recently shown.[18] However, despite the aforementioned interest on bimetallic Au-Ag NPs, only one example of a composite of Au-Ag bimetallic NPs included within a MTF has been reported.[19] Although the results presented by Chassagneux *et al.* are very interesting in terms of the NPs composition control, the SiO_2 used as support was only mesostructured (*i.e.* the pores were filled with the template) and, as a consequence, the application of the composites is very limited due to instability issues. TiO_2 as support represents a clear advantage in terms of chemical and mechanical stability[20] and can also provide new features to the composite, due to the well-known synergy between metals and semiconductors.[21] In fact, a recent article presented the promising photocatalytic activity of composites prepared by plasma deposition of Au-Ag bimetallic particles on top of a TiO_2 porous film prepared by magnetron sputtering.[22]

In this work, a two-step method to obtain bimetallic Au-Ag NPs entrapped inside TiO_2 MTF is presented. In a first step, Ag NPs were grown inside TiO_2 MTF by photoreduction and afterwards, a galvanic replacement reaction with Au (III) was used to produce Au-Ag bimetallic NPs. All reactions take place at room temperature conditions, making the process very simple. The Au-Ag bimetallic NPs – Ti_2O MTF composites were characterized by several techniques, and evaluated as catalysts for the reduction of 4-nitrophenol. The interplay among synthesis conditions, metallic loading and catalytic activity was evaluated, in order to better understand the potentiality of the composites.

Accepted Manuscript

This article is protected by copyright. All rights reserved.

Results and Discussion

Synthesis of bimetallic NPs inTiO_2 MTF

Bimetallic Au-Ag NPs were synthesized inside the pores of the TiO_2 mesoporous thin films. These films were prepared by dip coating, using a previously reported EISA based procedure, with Pluronic F127 as template agent.[23] The obtained TiO_2 MTF presented a pore diameter of 8 ± 1 nm (determined by TEM, see Figure S1, SI), a porosity of 34 % and a thickness of 180 ± 4 nm (both determined by XRR, Figure S2, SI).

The first step to generate the bimetallic NPs was the confinement of the Ag NPs inside the MTFs, through a two-step procedure, previously reported, comprising Ag^+ adsorption and UV induced photoreduction.[24] Two UV irradiation times (30 and 60 minutes) were tested, in order to vary the amount of Ag NPs incorporated within the oxide; samples are identified as Ag30 and Ag60 according to the time used for the procedure. After irradiation, a change in color can be observed in the TiO_2 MTFs, independently of the irradiation time used: the originally colorless MTFs turned brownish (see Figure S3a, SI). Such color change is a consequence of the Ag NPs formation. In fact, the UV–vis spectrum shows a broad absorption band with a maximum around 480 nm, which can be attributed to localized surface plasmon resonance (LSPR) band of the metallic Ag NPs. An increase in the intensity of the Ag LSPR band as a function of the irradiation time was observed, due to the formation of more Ag NPs inside the pores, as expected (see Figure S3b, SI).

After Ag NPs formation, a galvanic replacement reaction was used to obtain the bimetallic Ag-Au NPs. Since the $AuCl_4^-$ / Au standard reduction potential is at 0.99 V (vs SHE), while Ag^+ / Ag pair is at 0.80 V, the Ag NPs react with a $HAuCl_4$ solution to form metallic Au, according to the reaction presented in equation 1.

$$3Ag + AuCl_4^- \rightarrow Au + 3Ag^+ + 4Cl^- \quad (1)$$

As outlined, the galvanic replacement reaction consists of a redox process between a metal, employed as a sacrificial template (in this case Ag) and metal ions in solution (Au(III) in our experiments). The reduction potential between the Ag NPs and Au (III) is the driving force for the oxidation and dissolution of the Ag NPs, taking place in parallel with Au reduction, which deposits on the Ag NP. The galvanic replacement reaction has been widely employed in the synthesis of bimetallic NPs and offers a particularly effective and versatile approach, since allows tuning the composition and structure of the final particles.[25]

Accepted Manuscript

This article is protected by copyright. All rights reserved.

Thus, the Ag NP MTF composites were immersed for different times in a $HAuCl_4$ solution. Samples were denominated Ag*x*Au*y*, where *x* and *y* denote the reaction times in each step, measured in minutes.

After film immersion, a color change was observed, indicating that a reaction has occurred. Samples change their color from dark brown (the color coming from the supported Ag NPs) towards a pink color whose final tone depends on the reaction time, as can be seen in Figure 1d.

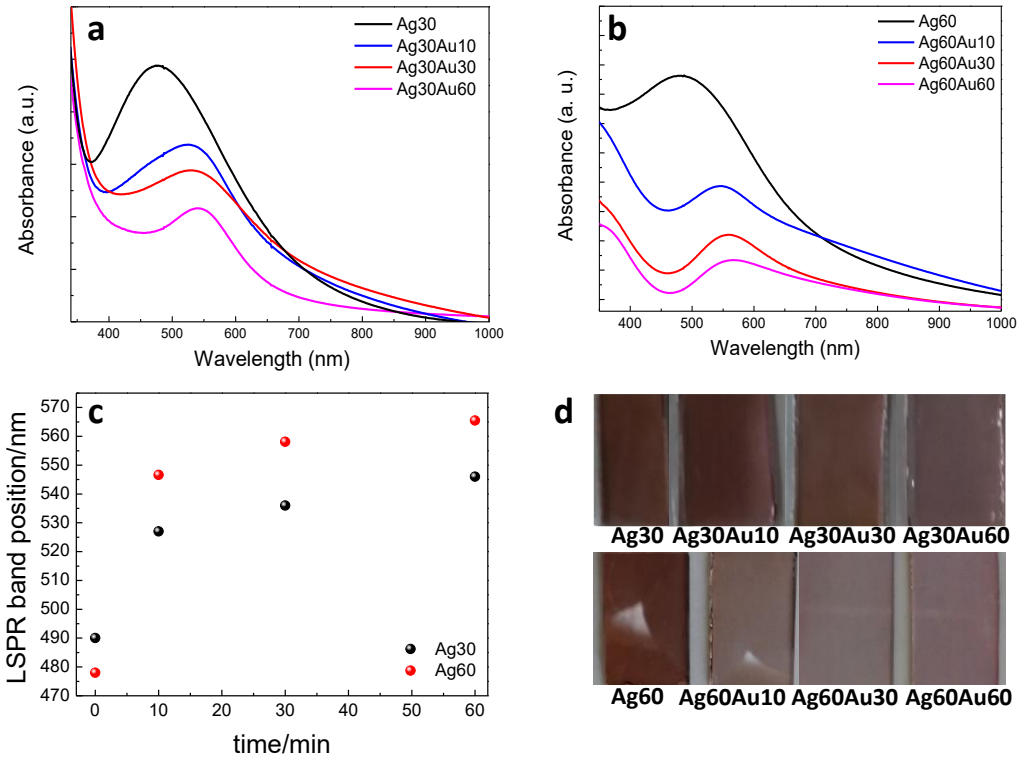

Figure 1. UV-visible spectra of samples **(a)** Ag30Au*y* and**(b)** Ag60Au*y*. **(c)** LSPR band position as a function of the reaction time for galvanic replacement. (**d**) Optical images of obtained samples.

This change in color was also followed by UV-vis spectroscopy, as shown in Figure 1a and Figure 1b. The first clear observation is that only a single LSPR band is present after the galvanic replacement, for all systems. Moreover, a shift in the LSPR peak from ~480 nm (corresponding to the Ag NPs) towards longer wavelengths is observed when the reaction time increases for both Ag30 and Ag60 samples. The band maximum position ad a function of galvanic replacement reaction time is presented in Figure 1c. Interestingly, after 60 minutes of reaction, the LSPR band's position is close to the one observed for Au NPs entrapped inside TiO_2 mesoporous films.[26] Both the presence of

Accepted Manuscript

This article is protected by copyright. All rights reserved.

only one LSPR band and its shift when the reaction time increases points towards the formation of alloyed rounded NPs, with an increasing amount of Au in the alloy as the reaction proceeds.[2b, 27]

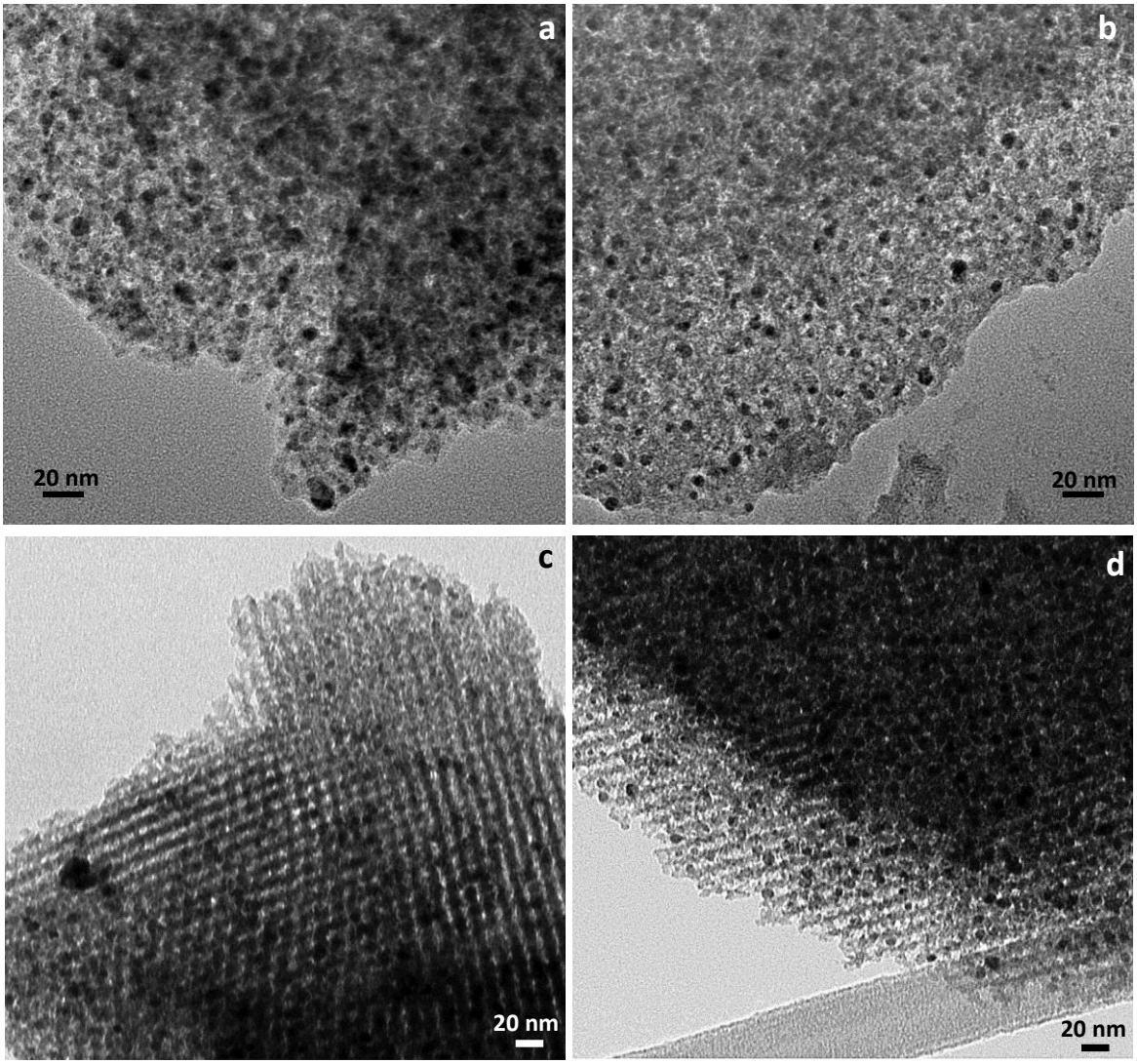

Figure 2 TEM images of (**a**) Ag30Au2.5, (**b**) Ag30Au30, (**c**) Ag60Au10 and (**d**) Ag60Au30 samples.

Figure 2 presents TEM images of selected Ag30Au*y* and Ag60Au*y* samples. The NPs can be seen as darker spots, included within the pores and well distributed along the sample. High resolution images confirm the absence of core-shell NPs, since this type of structures is not seen (Figure S4, SI). Thus, the images confirm UV-vis results that pointed towards the formation of a Ag-Au solid solution or alloy inside the TiO_2 MTF. Moreover, the average NPs size decreased from 7.3 ± 0.8 nm to 6.2 ± 0.7 nm for Ag30Au2.5 and Ag30Au30 samples respectively. This result is in agreement with the fact that three Ag atoms are replaced by one Au atom, with the consequent decrease in final

Accepted Manuscript

This article is protected by copyright. All rights reserved.

NPs volume. Similar results were obtained for the Ag60Auy system. The crystallinity of NPs was studied by grazing incidence XRD measurements (Figure S5, SI).A single and very broad peak can be seen in all Ag60Auy samples. This single peak appears at 38.2° (2θ) and can be assigned to the (111) reflection of the face-centered cubic (fcc) structure of both Au and Ag.[28] These results indicate that the obtained NPs are crystalline, a fact that is coincident with HRTEM observations (Figure S4, SI). However, the similarity of the characteristic lattice parameters of metallic Ag and Au (a = 4.0782 Å for Au and 4.0862 Å for Ag) and the small size of the NPs does not allow a complete characterization of the alloy by means of XRD.[29]

XPS was employed to determine the Au and Ag concentrations and the valence state of the metals in the samples. The obtained spectra in the Ag 3d and Au 4f regions are presented in Figure 3.

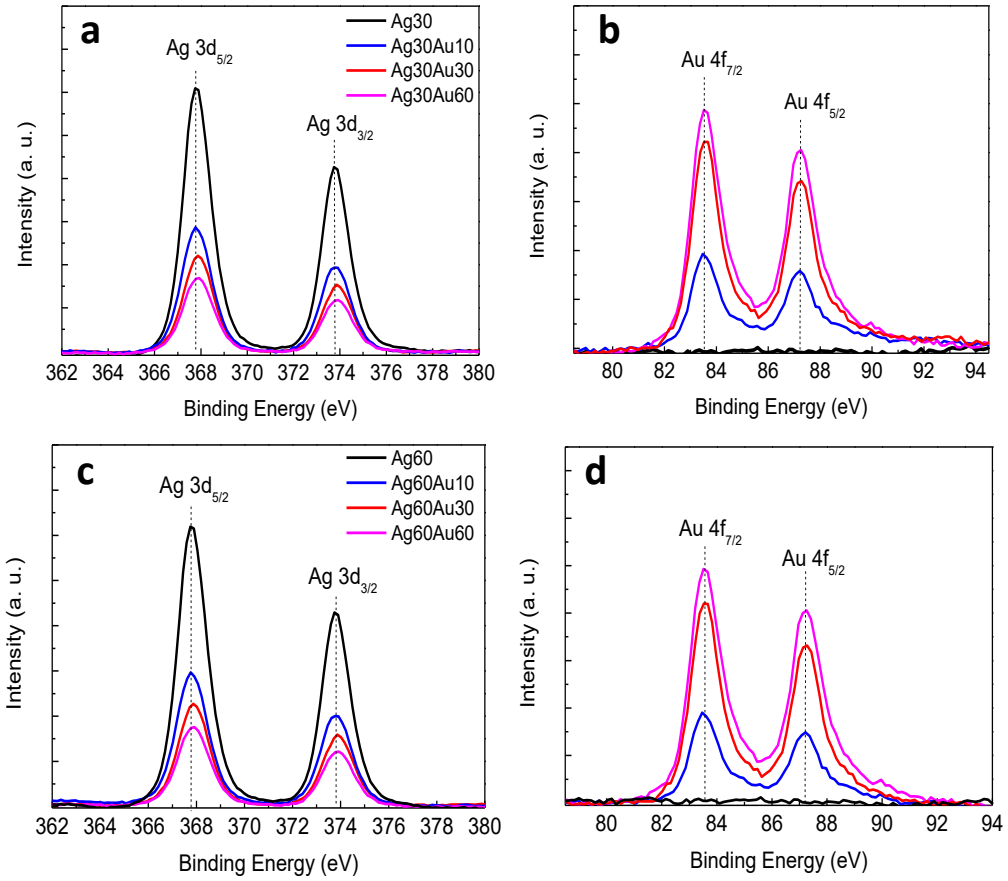

Figure 3.XPS spectra of Ag*x*Au*y* samples in the Ag 3d (**a** and **c**) and Au 4f regions (**b** and **d**).

Accepted Manuscript

This article is protected by copyright. All rights reserved.

10.1002/ejic.201901186

As expected, the intensity of Ag peaks decreases while the intensity of Au peaks increases as the galvanic replacement reaction proceeds. In the Ag region, the peaks at 367.9 and 373.9 eV can be assigned to the $3d_{5/2}$ and $3d_{3/2}$ levels of metallic Ag, respectively. On the other hand, the peaks around 83.6 and 87.3 eV can be assigned to the $4f_{7/2}$ and $4f_{5/2}$ levels of metallic Au, respectively. The observed positions are in agreement with the values obtained for other bimetallic systems reported in literature.[16a, 30] The composition ratio of the Ag and Au measured by XPS are reported in Table 1.

Table 1 Au:Ag Atomic ratios obtained from XPS spectra.

Sample	Au:Ag Atomic Ratio	Sample	Au:Ag Atomic Ratio
Ag60	0	Ag30	0
Ag60Au10	0.51	Ag30Au10	0.57
Ag60Au30	0.67	Ag30Au30	0.77
Ag60Au60	0.73	Ag30Au60	0.83

It can be seen that the Au:Ag atomic ratio increases with the galvanic replacement reaction time, for the two tested initial Ag concentrations. However, a no linear relationship with the time can be observed, indicating that the major part of the galvanic replacement occurs during the first 10 minutes of reaction.

Finally, XRR measurements were performed to determine changes in the film electronic density and accessibility after AuAg NPs formation inside of the pores.

Accepted Manuscript

This article is protected by copyright. All rights reserved.

10.1002/ejic.201901186

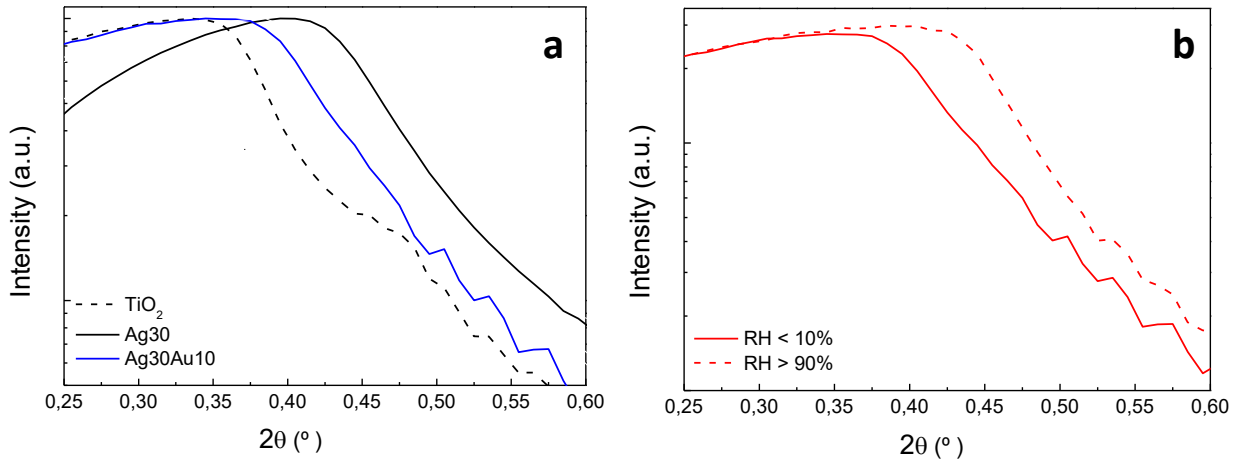

Figure 4 XRR results for (**a**) empty TiO_2, Ag30 and Ag30Au10 samples, obtained at low RH; and (**b**) Ag30Au30 sample measured at low and high RH.

Figure 4a shows the changes in the critical angle (θ_c) after the different synthesis steps. An increase in the θ_c is observed when TiO_2 pores are filled with Ag, due to the increase in the electronic density of the composite material, in accordance with previous results.[31] When the galvanic replacement takes place for 10 minutes, the θ_c of the obtained composite decreases. This observation is in agreement with the above mentioned decrease in the NPs volume due to the galvanic replacement reaction stoichiometry. When the reaction time was increased, the θ_c of Ag30Au*y* systems increases, but not exceeding θ_c of the system with only Ag NPs (see Figure S6, SI). The tendencies observed for the Ag60Au*y* systems (Figure S7) were equivalent, indicating that the behavior was not related to the original amount of Ag incorporated within the TiO_2. Interestingly, the XRR patterns confirm that the Ag NPs and Ag-Au NPs are deposited inside the TiO_2 MTF pores, since only one critical angle is observed, the one corresponding to the composite.

The reflectograms of the composites were also measured at low (<5%) and high (>95%) relative humidity, in order to characterize the accessible porosity after each reaction step. An example of the obtained results is presented in Figure 4b for Ag30Au30 sample. More information can be found in Figures S6 and S7, SI. In all cases, an increment in θ_c due to water condensation inside the pores is observed. Thus, all the synthesized composite samples displayed accessible porosity after NPs incorporation and can be used in applications that require the entrance of reagents inside the porous structure, as in catalysis.

Accepted Manuscript

This article is protected by copyright. All rights reserved.

Catalytic activity

The catalytic activity of the composites was studied using the well-known reduction of 4-nitrophenol (NIP) to 4-aminophenol, using $NaBH_4$as reductive agent.[32] For this purpose, pieces of the different samples were immersed in NIP solution and its degradation was followed by UV-visible spectrometry. In all cases, the reaction proceeds immediately after the introduction of the films in the reaction media[33] and a discoloration of the originally yellow NIP solution is observed. An example of the spectra evolution as a function of time is presented in Figure 5a. In contrast, when a TiO_2 film is immersed, under the same conditions, in the reaction mixture, no discoloration of the NIP solution is observed (Figure S8, SI). This result indicates that the metallic particles are the responsible of the catalytic activity.

Moreover, the stability of samples used for catalytic experiments was confirmed by EDS measurements (see Table S1, SI).

Accepted Manuscript

This article is protected by copyright. All rights reserved.

10.1002/ejic.201901186

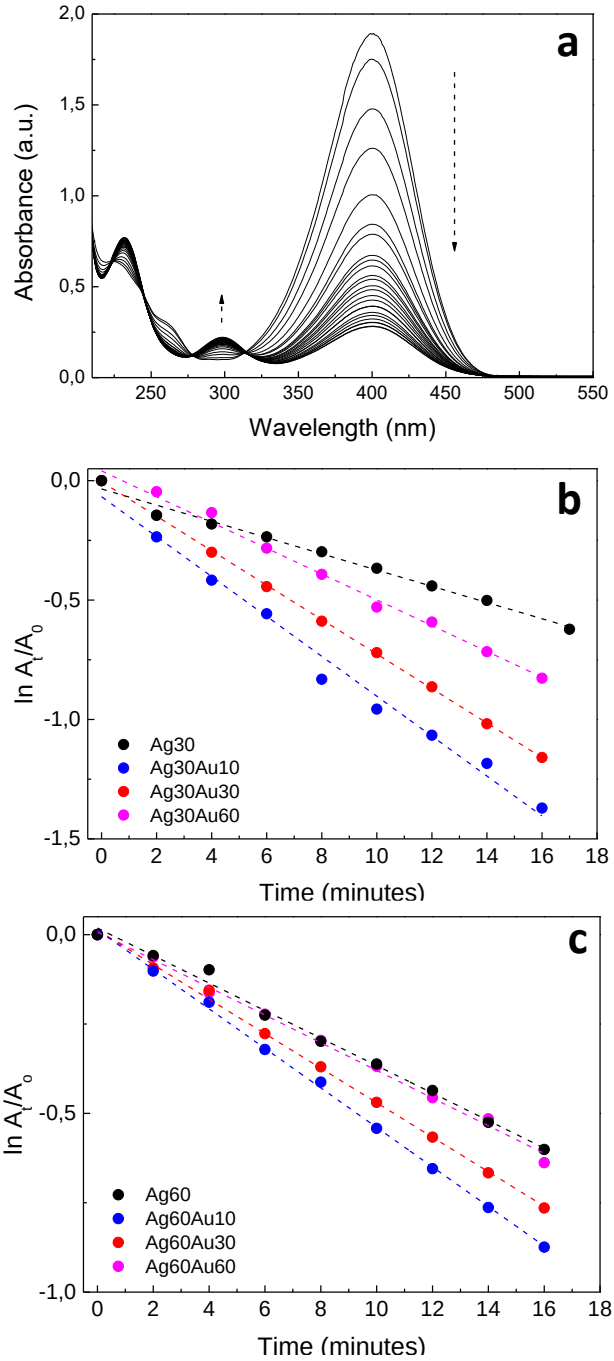

Figure 5 (a) Time-dependent UV–vis absorption spectra of the NIP reduction by $NaBH_4$ in presence of the Ag30Au10 sample. Plot of $\ln(A_t/A_0)$ as a function of time for the reaction catalyzed by (**b**) Ag30Au*y* and (**c**) Ag60Au*y* samples. Each group of data is presented with the correspondent linear fitting.

The reaction rate from 4-nitrophenol to 4-aminophenol can be adjusted according to a pseudo first-order kinetics, described by equation 2:

Accepted Manuscript

This article is protected by copyright. All rights reserved.

$ln(At/A_0) = -kt$ (2)

where k is the pseudo first-order rate constant, t is the reaction time and A_t and A_0 are the absorbance of NIP at λ = 400 nm at time t and 0, respectively.[34] The $ln(At/A_0)$ vs time charts for all tested samples are presented in Figure 5b and c, with the corresponding linear fittings. For all samples, a linear behavior is observed, corroborating the pseudo first-order kinetics. The slope of each linear adjustment corresponds to k, from which the apparent constant rate normalized per geometric area (k_{app}) was calculated dividing the k value by the geometric area of the sample used for each experiment. The obtained results are reported in Table 2.

Table 2 k_{app}values for the different tested samples

Sample	k_{app} / min^{-1} cm^{-2}	Sample	k_{app} / min^{-1} cm^{-2}
Ag30	0.033	Ag60	0.038
Ag30Au10	0.078	Ag60Au10	0.055
Ag30Au30	0.070	Ag60Au30	0.045
Ag30Au60	0.050	Ag60Au60	0.039

All tested composites present catalytic activity towards the 4-nitrophenol reduction to 4-aminophenol. However, the k_{app} values clearly depend on the composition of the samples. In particular, for both families, it can be seen that the catalytic activity of all the bimetallic composites is better than for the Ag NPs loaded TiO_2 MTF. This improvement in the catalytic activity of Ag-Au NPs in comparison with the Ag NPs has been previously observed[9, 16a, 32b, 35] and has been associated with electronic charge transfer effects between Ag and Au,[16a, 35d] changes in the metals atomic distribution on the surface[16a] and/or to the modification of the metals electronic structure.[9]
Moreover, larger k_{app} values were observed for Ag30Auy composites than for Ag60Auy ones. Additionally, for both Ag30 and Ag60 families, the larger k_{app} values were obtained for the bimetallic particles with lower Au content, *i.e.* Ag60Au10 and Ag30Au10 samples. Since the size and the composition of the NPs vary in each sample, it is not simple to analyze those variables separately. However, it seems that Au improves catalytic activity in low amounts and the inclusion of a higher concentration of this metal is counterproductive. The existence of an ideal Ag:Au ratio has been observed before, and was attributed to a complex interplay between the effects of surface

Accepted Manuscript

This article is protected by copyright. All rights reserved.

composition, the presence of interfaces with different characteristics and the NPs size.[28, 36] More detailed studies taking into account these factors are planned. However, it can be concluded that the Ag30Au10 system is the most effective for the catalytic degradation of NIP. Moreover, preliminary reuse experiments indicate a fair stability of this sample (see Figure S9, SI). More experiments are being conducted in order to understand and improve the catalyst stability.

Conclusions

In this work, the synthesis, characterization and catalytic efficiency of bimetallic Ag-Au NPs supported in TiO_2 MTF were presented. Ag-Au NPs – TiO_2 MTFs composites were synthesized by means of a two-step procedure that involves Ag photodeposition inside the TiO_2 MTF pores and the subsequent galvanic replacement by Au, which results in the formation of bimetallic structures inside the pores. All experiments were performed at room temperature, avoiding harsh reaction conditions.

UV-vis and TEM analysis proved that alloyed NPs were obtained inside the mesopores of the MTF. Moreover, by adjusting reaction times, both Ag and Au loading could be controlled, as demonstrated by XPS analysis. XRR results demonstrated that a portion of the mesoporosity remains accessible after the NPs synthesis, a feature that ensures the possible applications of the composites in any device that requires the contact between the NPs and the medium. As a first test, the catalytic activity of the composites towards 4-nitrophenol reduction by sodium borohydride was studied. The catalytic performance of the bimetallic systems was different for each of the tested composites, but in all cases the catalytic performance was better for the bimetallic composites than for the monometallic Ag NPs - MTF composites, in agreement with previously reported results for colloidal suspensions or powder supported bimetallic NPs.

The presented results demonstrate for the first time, to the best of our knowledge, the feasibility of producing bimetallic Au-Ag NPs inside mesoporous TiO_2 films, paving the way towards a wide variety of applications.

Experimental

TiO_2 Mesoporous Thin Films Synthesis

Accepted Manuscript

This article is protected by copyright. All rights reserved.

TiO_2 mesoporous thin films were produced by combining a sol−gel chemistry route with self-assembly of surfactant templates, using the strategy known as Evaporation Induced Self Assembly (EISA).[37] In a typical synthesis, Pluronic F127 ($PEO_{106}PPO_{70}PEO_{106}$, Sigma) was added to an ethanol solution of titanium tetrachloride ($TiCl_4$, Merck). Water was subsequently added under stirring. The final molar ratio $TiCl_4$:EtOH:F127:H_2O was 1:40:0.005:10.[23] Glass slides were used as substrates for the deposition of the films. The glass slides, previously washed with water, acetone, and ethanol, were dipped into the sol heated up to 32°C, and then extracted at a constant withdrawal rate of 2 $mm \cdot s^{-1}$, using a dip coater. Freshly prepared films were submitted to a stabilization process in several steps, as follows: 24 h in a chamber at 50 % Relative Humidity, 24 h in an oven at 60ºC, 24 h in an oven at 130ºC and a calcination for 2 h at 350ºC (heating rate: 1ºC·min^{-1}).

Metallic loading

Ag NPs were synthesized inside the MTF by adapting a previously reported procedure.[24] The films were immersed in a 0.087 M $AgNO_3$ solution, prepared in a 1:1 water:ethanol mixture for 10 minutes. Then, the $AgNO_3$ loaded films were irradiated with a UV lamp (15W), for 30 minutes (sample Ag30) or 60 minutes (sample Ag60) and finally washed with MilliQ water. The TiO_2 MTF loaded with Ag-Au bimetallic NPs were obtained by immersion of Ag30 or Ag60 samples in 3ml of 0.1 mM $HAuCl_4$ aqueous solution, for different times: 10, 30 and 60 minutes. Then, samples were washed with MilliQ water and dried under air flow. Samples were denominated Ag*x*Au*y*, where *x* and *y* denote the reaction times in each step, measured in minutes. As an example, Ag60Au30 sample was irradiated for 60 minutes to form the Ag NP and was subsequently immersed for 30 minutes in the Au (III) solution.

Characterization

UV-visible spectra were obtained using an Agilent 8453 UV-visible spectrophotometer. Pore structure and metallic loading were studied by Transmission Electron Microscopy (TEM) using a JEOL JEM-1400PLUS microscope equipped with a GATAN US1000 CCD camera and by high resolution TEM (HRTEM) using a CM 200 Philips microscope equipped with an ultratwin objective lens and an acceleration voltage of 200 kV (CAB−CNEA). TEM samples were prepared by scratching the films from the substrate and depositing the fragments onto carbon and Formvar coated Cu grids.

X-ray reflectometry (XRR) measurements were performed using a PanAnalytical Empyrean X-Ray diffractometer with a Cu Kα radiation source (1.54 Å). Films thicknesses, porosities and metallic

Accepted Manuscript

This article is protected by copyright. All rights reserved.

filling were determined from XRR data. Details about these calculations are presented in the Supporting Information. The same equipment was used to perform X-Ray diffraction (XRD) measurements using a 1° incident beam angle, a 0.38 mm divergence slit and a 10 mm mask. Diffraction patterns were collected from 29 to 42° (2θ) with a step size of 0.05° and time per step of 10 s.

X-ray photoelectron spectroscopy (XPS) data were recorded using a SPECS Sage HR 100 spectrometer equipped with a 100 mm mean radius PHOIBOS analyzer and a non-monochromatic X-ray source (Magnesium Kα line of 1253.6 eV energy and 250 W). Such source is placed perpendicular to the analyzer axis and was calibrated using the $3d_{5/2}$ line of Ag with a full width at half maximum (FWHM) of 1.1 eV. The selected resolution for the high resolution spectra was 15 eV of pass energy and 0.15 eV/step. All measurements were performed in an ultra-high vacuum chamber at a pressure around $8 \cdot 10^{-8}$mbar. An electron flood gun was used for charge neutralization. Measurements were conducted directly on the films, which were previously washed with absolute ethanol and cut into pieces of 1 cm^2. The spectral analysis was performed with CasaXPS 2.3.15dev87 software. Satellite removal and Shirley background subtraction were applied; binding energies were calibrated assigning 285 eV to the C 1s C-C peak and peaks were fitted with Gaussian-Lorentzian line shapes to determine the atomic percentages of the elements present in the samples.

Catalytic measurements

The catalytic activity of the composites towards 4-nitrophenol reduction was evaluated using UV–vis spectroscopy. For this purpose, a 3 mL quartz cuvette cell was used. 10 µL of an aqueous solution of 4-nitrophenol (0.01 M) and100 µL of a freshly prepared aqueous solution of $NaBH_4$ (0.5 M) were mixed with 2.5 mL of milliQ water. A piece of ~1 cm^2 of the sample was introduced in the cuvette filled with a reaction solution. The slide was positioned in such a way that it did not block the beam path. The absorbance of the solution was recorded in a scanning range of 200–800 nm, every two minutes until reaction completion.

Acknowledgments

The authors thank the financial support from ANPCyT (PICT 2012-0111 and 2015-0351) and CONICET (PIP 2012-00044CO). R.C.R. acknowledges CONICET for a postdoctoral scholarship. We thank M. C. Fuertes and M. M. Zalduendo for their assistance with XRD and XRR measurements, A. Martínez-Villacorta for TEM measurements and Luis Yate for XPS measurements. S.E. Moya thanks the

Accepted Manuscript

This article is protected by copyright. All rights reserved.

MAT2017-88752-R Retos project from the Ministerio de Economía, Industria y Competitividad, Gobierno de España.

References

[1] aK. L. Kelly, E. Coronado, L. L. Zhao, G. C. Schatz, *J. Phys. Chem. B* **2003**, *107*, 668–677; bG. A. Ozin, A. Arsenault, *Nanochemistry. A chemical approach to nanomaterials*, 1 ed., RSC Publishing Group, **2005**.

[2] aK. D. Gilroy, A. Ruditskiy, H.-C. Peng, D. Qin, Y. Xia, *Chem. Rev.* **2016**, *116*, 10414-10472; bM. B. Cortie, A. M. McDonagh, *Chem. Rev.* **2011**, *111*, 3713-3735.

[3] D. Alloyeau, C. Mottet, C. Ricolleau, *Nanoalloys: Synthesis, Structure and Properties*, Springer Science & Business Media, **2012**.

[4] R. Intartaglia, G. Das, K. Bagga, A. Gopalakrishnan, A. Genovese, M. Povia, E. Di Fabrizio, R. Cingolani, A. Diaspro, F. Brandi, *Phys. Chem. Chem. Phys.* **2013**, *15*, 3075-3082.

[5] X. Cao, N. Wang, S. Jia, L. Guo, K. Li, *Biosens. Bioelectron.* **2013**, *39*, 226-230.

[6] M. Laskowska, I. Kityk, M. Dulski, J. Jędryka, A. Wojciechowski, J. Jelonkiewicz, M. Wojtyniak, Ł. Laskowski, *Nanoscale* **2017**, *9*, 12110-12123.

[7] J. Rick, M.-C. Tsai, B. J. Hwang, *Nanomaterials* **2016**, *6*, 5.

[8] J. Cheng, X. Gu, X. Sheng, P. Liu, H. Su, *J. Mater. Chem. A* **2016**, *4*, 1887-1894.

[9] A. Monga, B. Pal, *New J. Chem.* **2015**, *39*, 304-313.

[10] C. Gao, Y. Hu, M. Wang, M. Chi, Y. Yin, *J. Am. Chem. Soc.* **2014**, *136*, 7474-7479.

[11] aK. Sapkota, S. S. Han, *New J. Chem.* **2017**, *41*, 5395-5402 ; bE. N. Saw, V. Grasmik, C. Rurainsky, M. Epple, K. Tschulik, *Faraday Discuss.* **2016**, *193*, 327-338; cS. K. Singh, A. K. Singh, K. Aranishi, Q. Xu, *J. Am. Chem. Soc.* **2011**, *133*, 19638-19641.

[12] aT. Zhang, F. Zhou, L. Hang, Y. Sun, D. Liu, H. Li, G. Liu, X. Lyu, C. Li, W. Cai, *J. Mater. Chem. C* **2017**, *5*, 11039-11045; bP. Khurana, S. Thatai, S. Prasad, S. Soni, D. Kumar, *Microchem. J.* **2016**, *124*, 819-823; cY. Yang, J. Liu, Z.-W. Fu, D. Qin, *J. Am. Chem. Soc.* **2014**, *136*, 8153-8156; dJ.-F. Li, Y.-J. Zhang, S.-Y. Ding, R. Panneerselvam, Z.-Q. Tian, *Chem. Rev.* **2017**, *117*, 5002-5069.

[13] R. J. White, R. Luque, V. L. Budarin, J. H. Clark, D. J. Macquarrie, *Chem. Soc. Rev.* **2009**, *38*, 481-494.

[14] aJ. Liu, S. Zou, L. Xiao, J. Fan, *Catal. Sci. Technol.* **2014**, *4*, 441-446; bN. Pal, A. Bhaumik, *RSC Advances* **2015**, *5*, 24363-24391.

[15] aD. Gu, F. Schuth, *Chem. Soc. Rev.* **2014**, *43*, 313-344; bC. T. Kresge, W. J. Roth, *Chem. Soc. Rev.* **2013**, *42*, 3663-3670; cG. J. A. A. Soler-Illia, C. Sanchez, B. Lebeau, J. Patarin, *Chem. Rev.* **2002**, *102*, 4093-4138.

[16] aS. Sareen, V. Mutreja, B. Pal, S. Singh, *Appl. Surf. Sci.* **2018**, *435*, 552-562; bC.-W. Yen, M.-L. Lin, A. Wang, S.-A. Chen, J.-M. Chen, C.-Y. Mou, *J. Phys. Chem. C* **2009**, *113*, 17831-17839; cM. Zienkiewicz-Strzałka, A. Deryło-Marczewska, S. Pikus, *Microporous Mesoporous Mater.* **2016**, *227*, 228-241; dX. Liu, A. Wang, X. Yang, T. Zhang, C.-Y. Mou, D.-S. Su, J. Li, *Chem. Mater.* **2009**, *21*, 410-418; eZ. Qu, G. Ke, Y. Wang, M. Liu, T. Jiang, J. Gao, *Appl. Surf. Sci.* **2013**, *277*, 293-301; fA. Wang, Y.-P. Hsieh, Y.-F. Chen, C.-Y. Mou, *J. Catal.* **2006**, *237*, 197-206; gA.-Q. Wang, C.-M. Chang, C.-Y. Mou, *J. Phys. Chem. B* **2005**, *109*, 18860-18867.

[17] P. Innocenzi, L. Malfatti, *Chem. Soc. Rev.* **2013**, *42*, 4198-4216.

[18] aP. C. Angelomé, M. C. Fuertes, in *Handbook of Sol-Gel Science and Technology* (Eds.: L. Klein, M. Aparicio, A. Jitianu), Springer International Publishing, Cham, **2018**, pp. 2507-2533 ; bP. C. Angelomé, L. M. Liz-Marzán, *J. Sol-Gel Sci. Technol.* **2014**, *70*, 180-190; cP. Innocenzi, L. Malfatti, *J. Nanopart. Res.* **2018**, *20*, 167.

Accepted Manuscript

This article is protected by copyright. All rights reserved.

[19] F. Chassagneux, L. Bois, J.-P. Simon, C. Desroches, A. Brioude, *J. Mater. Chem.* **2011**, *21*, 11947-11955.

[20] S. Alberti, P. Steinberg, G. Gimenez, H. Amenitsch, G. Ybarra, O. Azzaroni, P. C. Angelomé, G. J. A. A. Soler-Illia, *Langmuir* **2019**, *35*, 6279-6287.

[21] aM. Diak, M. Klein, T. Klimczuk, W. Lisowski, H. Remita, A. Zaleska-Medynska, E. Grabowska, *Applied Catalysis B: Environmental* **2017**, *200*, 56-71; bD. Tsukamoto, A. Shiro, Y. Shiraishi, Y. Sugano, S. Ichikawa, S. Tanaka, T. Hirai, *Acs catalysis* **2012**, *2*, 599-603.

[22] A. Müller, S. Peglow, M. Karnahl, A. Kruth, H. Junge, V. Brüser, C. Scheu, *Nanomaterials* **2018**, *8*, 502.

[23] E. L. Crepaldi, G. J. A. A. Soler-Illia, D. Grosso, F. Cagnol, F. Ribot, C. Sánchez, *J. Am. Chem. Soc* **2003**, *125*, 9770-9786.

[24] E. D. Martínez, M. G. Bellino, G. J. A. A. Soler-Illia, *ACS Appl. Mater. Interfaces* **2009**, *1*, 746-749.

[25] aX. Xia, Y. Wang, A. Ruditskiy, Y. Xia, *Adv. Mater.* **2013**, *25*, 6313-6333; bA. G. M. da Silva, T. S. Rodrigues, S. J. Haigh, P. H. C. Camargo, *Chem. Comm.* **2017**, *53*, 7135-7148.

[26] M. M. Zalduendo, J. Langer, J. J. Giner-Casares, E. B. Halac, G. J. A. A. Soler-Illia, L. M. Liz-Marzán, P. C. Angelomé, *J. Phys. Chem. C* **2018**, *122*, 13095-13105.

[27] K. S. Shin, J. H. Kim, I. H. Kim, K. Kim, *J. Nanopart. Res.* **2012**, *14*, 735.

[28] H. Zhang, J. Okuni, N. Toshima, *J. Colloid Interface Sci.* **2011**, *354*, 131-138.

[29] A. Guiet, T. Unmüssig, C. Göbel, U. Vainio, M. Wollgarten, M. Driess, H. Schlaad, J. Polte, A. Fischer, *ACS Appl. Mater. Interfaces* **2016**, *8*, 28019-28029.

[30] R. Liu, J. Guo, G. Ma, P. Jiang, D. Zhang, D. Li, L. Chen, Y. Guo, G. Ge, *ACS Appl. Mater. Interfaces* **2016**, *8*, 16833-16844.

[31] M. Fuertes, M. Marchena, M. Marchi, A. Wolosiuk, G. Soler-Illia, *Small* **2009**, *5*, 272-280.

[32] aS. Wunder, F. Polzer, Y. Lu, Y. Mei, M. Ballauff, *J. Phys. Chem. C* **2010**, *114*, 8814-8820; bP. Zhao, X. Feng, D. Huang, G. Yang, D. Astruc, *Coord. Chem. Rev.* **2015**, *287*, 114-136.

[33] I. L. Violi, A. Zelcer, M. M. Bruno, V. Luca, G. J. Soler-Illia, *ACS Appl. Mater. Interfaces* **2015**, *7*, 1114-1121.

[34] aM. M. Kumari, J. Jacob, D. Philip, *Spectrochimica Acta Part A: Molecular and Biomolecular Spectroscopy* **2015**, *137*, 185-192; bT.-H. Park, H. Lee, J. Lee, D.-J. Jang, *RSC Advances* **2017**, *7*, 7718-7724.

[35] aL. Liu, A. Corma, *Chem. Rev.* **2018**, *118*, 4981-5079; bJ. F. Gomes, A. C. Garcia, C. Pires, E. B. Ferreira, R. Q. Albuquerque, G. Tremiliosi-Filho, L. H. S. Gasparotto, *J. Phys. Chem. C* **2014**, *118*, 28868-28875; cX. Huang, X. Wang, X. Wang, X. Wang, M. Tan, W. Ding, X. Lu, *J. Catal.* **2013**, *301*, 217-226; dH. Zhang, N. Toshima, *Applied Catalysis A: General* **2012**, *447*, 81-88; eH. Zhang, N. Toshima, *Catalysis Science & Technology* **2013**, *3*, 268-278.

[36] S. Tang, S. Vongehr, X. Meng, *J. Mater. Chem.* **2010**, *20*, 5436-5445.

[37] C. J. Brinker, Y. Lu, A. Sellinger, H. Fan, *Adv. Mater.* **1999**, *11*, 579-585.

Accepted Manuscript

This article is protected by copyright. All rights reserved.